Xue and Xie
EURASIP Journal on Advances in Signal Processing (2023) 2023:88
https://doi.org/10.1186/s13634-023-01052-9

EURASIP Journal on Advances in Signal Processing

RESEARCH

Open Access

Partial response continuous phase modulation with a prolate spheroidal wave function for compass system in the S-band

Rui Xue[1] and Mingming Xie[1*]

*Correspondence: xiemingming0215@hotmail.com

[1] College of Information and Communication Engineering, Harbin Engineering University, Harbin, China

Abstract

Continuous phase modulation (CPM) has the characteristics of high power efficiency, spectral efficiency, and less out-of-band radiation, which is very suitable for the Compass S-band (2483.5–2500 MHz) with limited power and bandwidth. However, as more and more navigation systems share the S-band, the mutual interference between different systems is gradually increasing, and the compatibility of CPM signals with rectangular or raised cosine pulses needs to be further improved. To enhance the navigation performance and compatibility of current CPM candidate signals, we propose to apply continuous phase modulation with prolate spheroidal wave function (CPM-PSWF) to S-band navigation. The proposed modulation scheme selects PSWF with excellent time-frequency energy aggregation and flexible time-bandwidth product as the frequency pulse function of CPM. Then, the influence of key modulation parameters such as M, L, h, and C on CPM-PSWF power spectral density is analyzed, and a specific partial-response CPM-PSWF signal is proposed as the S-band candidate navigation signal. Finally, the navigation performance evaluation criteria are derived, and the proposed signal scheme and existing candidate schemes are comprehensively evaluated. Theoretical analysis and simulation results indicate that compared with CPM with B*M*2RC(8), cos-phase binary offset carrier (BOCc(4,4)), sin-phase binary offset carrier (BOCs(4,4)), minimum shift keying-BOCs (MSK-BOCs(4,4)) and binary offset carrier (BPSK(8)), the proposed signal scheme not only delivers exceptional spectral performance but also exhibits superior performance in code tracking accuracy and multipath suppression. In addition, in the acquisition and tracking phase, compared with other candidate signals except for BOCc(4,4), the mutual interference between the proposed signal scheme and most S-band signals is the lowest, which is easier to realize the compatibility of the Compass system with IRNSS, Galileo, and Globalstar systems.

Keywords: S-band, Modulation waveform, CPM-PSWF, Compatibility

1 Introduction

With the continuous evolution of global navigation satellite systems (GNSSs) and regional navigation satellite systems, L-band (1164–1300 MHz, 1559–1610 MHz) navigation signals are expected to exceed 400 in 2030 and there will be as many as 160 space-based navigation satellites [1]. The spectra of GPS, Galileo, GLONASS, and Compass systems in the L-band partially overlap or completely overlap, resulting in inevitable radio frequency interference between systems, and the problem of L-band wireless spectrum compatibility is becoming increasingly serious [2, 3]. Based on the nonrenewable nature of spectrum resources, exploring new frequency bands may be an effective solution to the above problems [4, 5].

To alleviate the congestion of L-band GNSS signals, the International Telecommunication Union (ITU) allocates the S-band (2483.5–2500 MHz) to radio determination satellite service (RDSS). The ratio navigation satellite service (RNSS) is a subset of the RDSS, so the S-band can also be used for satellite navigation services [6–8]. Compared with other GNSS service bands, the frequency range of the S-band can realize antenna sharing with ground communication services with a frequency range above 2.5 G. Realizing hardware reuse with mobile communication is easier, which is conducive to combining navigation and positioning services and mobile communication [9, 10]. Compared with the L-band, the S-band is less affected by the ionosphere and exhibits relatively small multipath error and phase noise [11, 12]. In particular, the combination of S-band and L-band measurements can effectively reduce ionospheric error, facilitate the resolution of integer ambiguity, improve positioning accuracy, and increase the diversity of satellite navigation services [13].

Based on the above excellent characteristics, the research and development of S-band resources have attracted wide attention from scholars and system suppliers. The Indian regional navigation satellite system (IRNSS) has used the S-band to transmit navigation signals [14]. The Globalstar communications satellite system also uses the S-band to broadcast voice services for users with a signal known as SRC(0.2,1) [15]. Europe and South Korea also considering using the S-band for the future Galileo system and Korean Positioning System (KPS) [16, 17]. For the Compass system, the research and development of the S-band can effectively improve its navigation spectrum occupancy rate, enhance international competitiveness, and avoid being in a passive position in frequency in the future. At present, the Compass system uses the S-band to broadcast RDSS signals [18].

The signal modulation method is the core part of the GNSS signal system design, which has an important influence on the code tracking accuracy, anti-multipath ability, and compatibility of the system. However, the effective bandwidth of the S-band is only 16.5 MHz, with very strict requirements for transmitting signals in such a narrow bandwidth. How to make full use of the S-band 16.5 MHz bandwidth resources while taking into account the signal compatibility constraints and navigation performance has become the focus of S-band modulation method research [19].

Galileo proposed several S-band candidate signals including composite binary offset carrier (CBOC(6,1,1/11)), binary offset carrier (BPSK(1), BPSK(4) and BPSK(8)) signals [20, 21]. IRNSS also utilizes the S-band to provide navigation and positioning services for users. The signals of the IRNSS include BPSK(1) and sin-phase binary offset carrier (BOCs(5,2)), which are used for standard positioning services and restricted services, respectively [14, 22]. BOCs(5,2), cos-phase binary offset carrier (BOCc(4,4)), BOCs(3,1), and BPSK(n) (n=1,4,5,8) are also recommended as candidate signals for the KPS in the S-band [17]. For the Compass system, some scholars have proposed BOCc(4,4), BOCs(4,4), and BPSK(8) as candidate signals in the S-band [23, 24].

BPSK and BOC are discontinuous phase modulations, resulting in excessively high spectral sidelobes. These modulation methods not only consume a significant amount of spectrum resources but also cause great interference for adjacent signals [25, 26]. PSWF and orthogonal frequency division multiplexing (OFDM) are considered to be applied in the S-band to achieve superior anti-multipath and compatibility [19, 20, 27], but their time-domain waveforms are not-constant envelopes. Non-constant envelope signals are prone to nonlinear distortion after passing through high-power amplifiers. Therefore, constant envelope and continuous phase characteristics are of great significance in the design of S-band signals.

CPM exhibits characteristics such as constant envelope, continuous phase, excellent spectral performance, and less out-of-band radiation, which is very suitable for S-band with limited power and bandwidth [28]. Minimum frequency shift keying-binary offset carrier (MSK-BOCs(4,4)) modulation has been considered for the S-band of the Compass system, which has higher compatibility and tracking accuracy than BPSK modulation and BOC modulation [23]. Lei Wang et al. discussed the application of spread spectrum MSK (SSMSK) in S-band RDSS, and the research results showed that SSMSK had better performance than BPSK in terms of acquisition, tracking, and user capacity [29]. In fact, MSK is a special CPM subclass, but the performance is not optimal. By selecting the frequency pulse function, correlation length, base number, and modulation index of the CPM signal, an infinite variety of CPM signals can be formed.

To better meet the requirements of the S-band, a specific CPM signal named BM2RC(8) is proposed. BM2RC(8) can meet the requirements of S-band compatibility constraints and has more advantages than BPSK(8), BOCs(4,4), and MSK-BOCs(4,4) in code tracking accuracy, anti-multipath ability, and anti-interference ability [30, 31]. Due to the excellent spectral performance of CPM modulation, Fujian Ma et al. regard CPM modulation as a general modulation scheme for L, S, and C multi-band navigation. BM2RC modulation is recommended as a candidate scheme for S-band, and the side lobe of the modulation is significantly smaller than that of BOC modulation [32]. Yanbo Sun has optimized the modulation parameters of CPM signals for future GNSS. For bands with strictly limited out-of-band transmission power, two CPM subclasses of BM2RC with half-integer or integer h greater than 1 and QM2RC with h=0.5 or h=1 are recommended as solutions for single main lobe and multi-main lobe GNSS signals, because their fast attenuation side lobe can effectively reduce the degree of signal distortion caused by non-ideal filtering [33]. Table 1 summarizes the main signal modulation parameters of the S-band systems.

The S-band bandwidth is narrow, and many navigation signals share this band. Interference between the systems is inevitable, and an excellent modulation method is needed to achieve good compatibility. Different frequency pulse signals determine the different spectral and navigation performance of CPM signals. The traditional recommended CPM waveform, such as MSK or BM2RC, their frequency pulse signals are rectangular pulses or raised cosine pulses, and their navigation performance and compatibility have great room for improvement. The zero-order PSWF waveform has excellent characteristics such as optimal time-frequency energy concentration and flexible change of time-bandwidth product.

Table 1 Signal modulation parameters of S-band systems

Types	System	Center frequency (MHz)	Modulation type	Chip rate (Mcps)	Subcarrier frequency (MHz)
Space based	Globalstar	2491.75	SRC(0.2,1)	1.2288	–
	IRNSS	2492.028	SPS: BPSK(1)	1.023	–
			RS: BOCs(5,2)	2.046	5.115
Planned signal	Galileo candidate	2492.028	CBOC(6,1,1/11)	1.023	6.138
			BPSK(n) (n=1,4,8)	$n \times 1.023$	–
	KPS candidate	2492.028	BOCs(5,2)	2.046	5.115
			BOCc(4,4)	4.092	4.092
			BOCs(3,1)	1.023	3.069
			BPSK(n) (n=1,4,5,8)	$n \times 1.023$	–
	Compass candidate	2492.028	BM2RC(8)	8.184	-
			BOCc(4,4)	4.092	4.092
			BOCs(4,4)	4.092	4.092
			MSK-BOC(4,4)	4.092	4.092
			BPSK(8)	8.184	–

Moreover, it has been proven that the performance of PSWF as the baseband signal waveform of a multi-carrier communication system is superior to that of a rectangular pulse signal [34]. It is worth exploring and studying whether the zero-order PSWF waveform as the frequency pulse function of CPM can improve the signal performance of existing S-band CPM signals. No public report on the use of this modulation method in the S-band and the evaluation of navigation performance has been found. The main contributions of this paper can be summarized as follows

(1) Modulation waveform is related to navigation performance. Based on the S-band characteristics and the excellent spectral characteristics of CPM-PSWF, this paper explores the application of CPM-PSWF modulation in the Compass system S-band.

(2) Compatibility and navigation performance are the key considerations in S-band signal design. Based on the PSD and implementation complexity of CPM-PSWF, this paper proposes a specific partial-response CPM-PSWF signal as a candidate navigation scheme for S-band.

(3) The proposed signal scheme is compared with the existing S-band candidate signals of the Compass system. The simulation results show that the proposed signal has fast out-of-band attenuation, excellent inter-system compatibility, optimal code tracking accuracy, and anti-multipath performance.

(4) The proposed CPM-PSWF modulation scheme can provide new ideas and references for future S-band satellite navigation signal design.

The rest of this paper is organized as follows: Sect. 2 describes the mathematical model and PSD function of the CPM-PSWF signal and studies the influence of different CPM-PSWF parameters on the PSD characteristics. Navigation performance evaluation criteria are introduced in Sect. 3. In Sect. 4, the proposed CPM-PSWF signal and other Compass S-band candidate signals are comprehensively evaluated and analysed. Finally, we conclude the paper in Sect. 5.

2 CPM-PSWF signal model

2.1 Mathematical model of the CPM-PSWF signal

Prolate spheroidal wave functions are a set of nonsinusoidal functions introduced by Selpian D. These functions possess remarkable features, including perfect time-frequency energy concentration, flexible and controllable time-bandwidth product, completeness, and orthogonality [35, 36]. Under the parameters, the zero-order PSWF signal is a set of PSWF signals with the best time-frequency energy concentration [37]. The frequency pulse function of the CPM signal has an important influence on its spectral performance. The smoother the time-domain waveform of the frequency pulse function is, the faster the sidelobe attenuation in the signal power spectrum and the more compact the signal spectrum. Therefore, utilizing the zero-order PSWF signal as the frequency pulse function of CPM is anticipated to enhance the navigation performance and compatibility of the existing CPM signals.

The principle diagram of CPM-PSWF signal generation is shown in Fig. 1. First, the zero-order PSWF $\beta_0(C,t)$ is selected as the frequency pulse function of CPM-PSWF. Then, $\beta_0(C,t)$ is integrated and normalized to obtain the phase pulse function $q(t)$. Next, by calculating the product of modulation parameter $2\pi h$, information symbol sequence α_i, and phase pulse function $q(t)$, the time-varying phase $\varphi(t,\alpha)$ is obtained. Finally, the CPM-PSWF signal $s(t,\alpha)$ is obtained by carrier phase modulation.

The time-domain expression of the CPM-PSWF signal is as follows [38]:

$$s(t,\alpha) = \sqrt{\frac{2E}{T}}\cos(2\pi f_0 t + \varphi(t,\alpha) + \varphi_0) \tag{1}$$

where E is the symbol energy, T is the symbol period, f_0 is the carrier frequency, φ_0 is the initial phase, and $\varphi(t,\alpha)$ is the time-varying phase of the information carrier expressed as:

$$\varphi(t,\alpha) = 2\pi h \sum_{i=-\infty}^{+\infty} \alpha_i q(t-iT) \quad nT \le t \le (n+1)T \tag{2}$$

where h denotes the modulation index, α_i is the sequence of information symbols, $\alpha_i \in \{\pm 1, \pm 3, \ldots, \pm(M-1)\}$, M is the base number, and $q(t)$ is the phase pulse function, which can be obtained by integrating $\beta_0(C,t)$. However, $q(t)$ needs to be normalized to

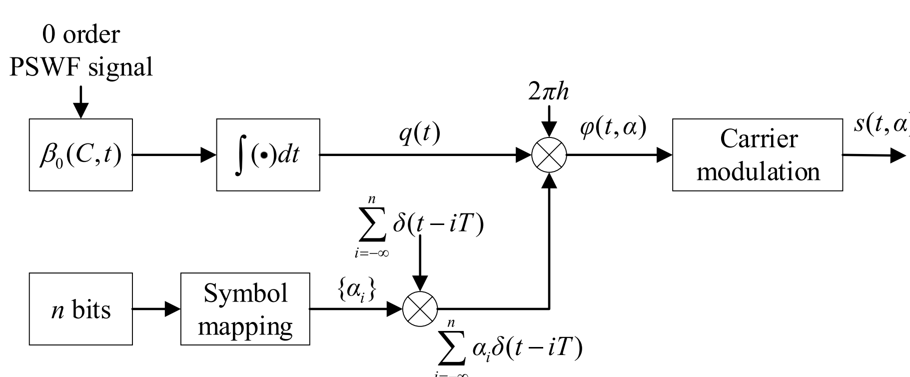

Fig. 1 CPM-PSWF signal generator scheme

make it monotonically increasing, and the maximum value is 0.5. The expression of $q(t)$ is:

$$q(t) = \begin{cases} 0 & t < 0 \\ \int_0^t \beta_0(C,\tau)d\tau & 0 \le t \le LT \\ 1/2 & t > LT \end{cases} \tag{3}$$

where $\beta_0(C,t)$ represents the zero-order PSWF, and the time-domain waveform of the zero-order PSWF and the phase pulse function are shown in Fig. 2. L is the correlation length, where $L = 1$ corresponds to a full response CPM-PSWF signal and $L > 1$ to a partial response CPM-PSWF signal. The integral equation expression of the zero-order PSWF is as follows:

$$\int_{-T/2}^{T/2} \beta_0(C,\tau)\frac{\sin\Omega(t-\tau)}{\pi(t-\tau)}d\tau = \lambda(C)\beta_0(C,\tau) \tag{4}$$

where $\beta_0(C,t)$ is the PSWF, which is band-limited to $[-\Omega, \Omega]$ and concentratedly distributed in the time domain $[-T/2, T/2]$, $C = T\Omega$ is the time-bandwidth product, which represents the degree of freedom of the system design, and λ is the eigenvalue corresponding to $\beta_0(C,\tau)$, The closed solution of the equation is difficult to solve directly. In this paper, the approximate solution is obtained by using the numerical method proposed by B. Parr [39].

2.2 CPM-PSWF PSD function

The PSD of the GNSS navigation signal has a profound impact on the code tracking performance, anti-multipath ability, anti-interference ability, and compatibility of the signal. Combined with the existing spectrum analysis method of the CPM signal and the characteristics of the PSWF signal, the PSD of the CPM-PSWF signal is analysed by the autocorrelation function. When the occurrence probabilities of all input information symbols are equal, the CPM-PSWF autocorrelation function can be calculated as [28]:

$$R(\tau) = \frac{1}{T}\int_0^T \prod_{k=1-L}^{\lfloor\tau/T\rfloor} \frac{1}{M}\frac{\sin(2\pi hM(q(t+\tau-kT)-q(t-kT)))}{\sin(2\pi h(q(t+\tau-kT)-q(t-kT)))}dt \tag{5}$$

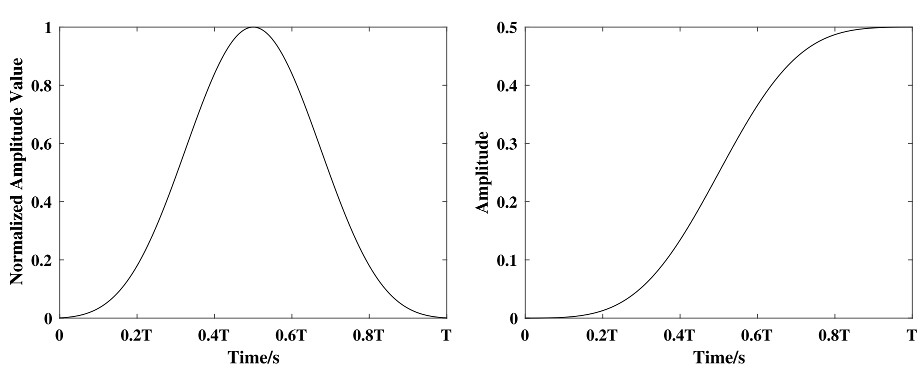

(a) Frequency pulse function (b) Phase pulse function

Fig. 2 Normalized zero-order PSWF frequency and phase pulse functions where $\lfloor . \rfloor$ denotes the downward integer function and τ is the correlation time. According to the Wiener-Khinchin theorem, the PSD of the CPM-PSWF signal is expressed as follows:

$$\begin{aligned} P(f) = 2(&\int_0^{LT} R(\tau)\cos(2\pi f\tau)d\tau) \\ &+ \frac{1-\xi(jh)\cos(2\pi fT)}{1+\xi^2(jh)-2\xi(jh)\cos(2\pi fT)}\int_{LT}^{(L+1)T} R(\tau)\cos(2\pi f\tau)d\tau \\ &- \frac{\xi(jh)\sin(2\pi fT)}{1+\xi^2(jh)-2\xi(jh)\cos(2\pi fT)}\int_{LT}^{(L+1)T} R(\tau)\sin(2\pi f\tau)d\tau \end{aligned} \tag{6}$$

with $\xi(jh) = \sin(M\pi h)/(M\sin(\pi h))$. Obviously, when M, h and L are fixed, the PSD of the CPM-PSWF signal is mainly affected by the phase pulse function $q(t)$, which is closely related to the frequency pulse function $\beta_0(C,t)$. Therefore, the nature of the frequency pulse function largely determines the spectral characteristics of the CPM-PSWF signal.

The PSD of the CPM-PSWF signal under different parameter conditions is shown in Fig. 3. Figure 3a depicts the influence of different modulation indices h on the PSD of the CPM-PSWF signal. The CPM-PSWF signal can exhibit spectral splitting characteristics similar to those of the BOC signal in the case of $h > 1$, and an increase in h tends to keep the main lobe of the CPM-PSWF PSD away from the carrier frequency. Figure 3b illustrates the effect of different correlation lengths L on the CPM-PSWF performance. It is clearly

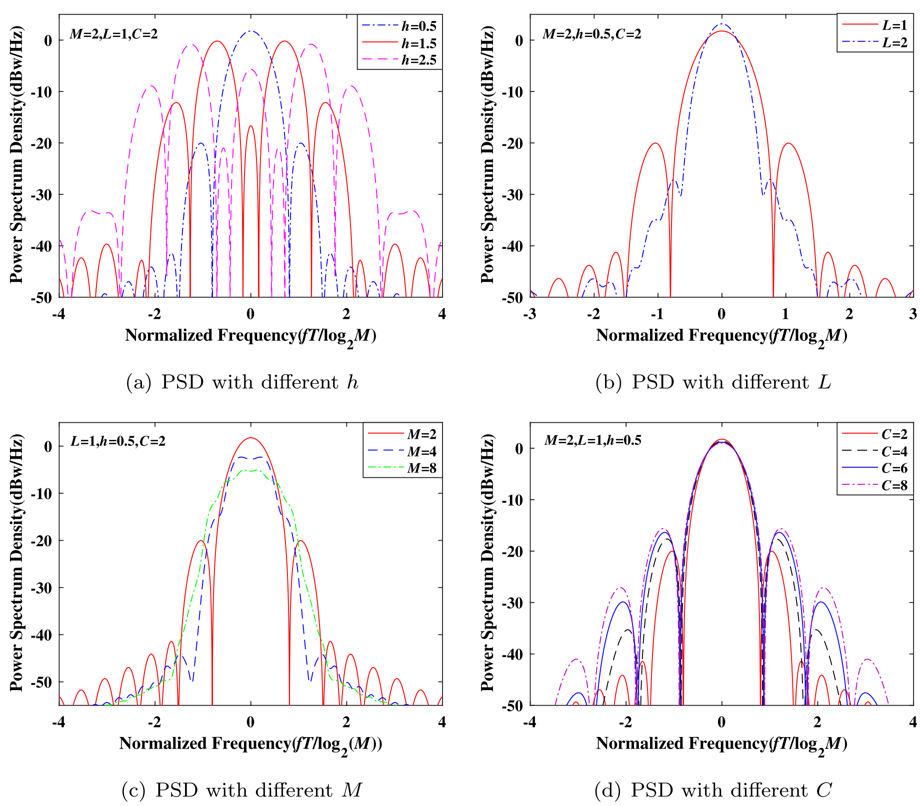

(a) PSD with different h (b) PSD with different L

(c) PSD with different M (d) PSD with different C

Fig. 3 PSD of the CPM-PSWF signal with different modulation parameters shown that CPM-PSWF signals with longer L can help concentrate more power on the signal main lobe, thus achieving better performance within a certain bandwidth. At the same time, the power spectrum sidelobe amplitude is effectively reduced, and interference to other signals in the same frequency band is smaller. Considering that the S-band bandwidth resources are limited and the compatibility requirements are high, the CPM-PSWF signal with $L > 1$ is selected.

Figure 3c shows the influence of different M values on the PSD of the CPM-PSWF signal. It can be seen that the larger M is, the faster the side lobe roll-off rate of the PSD of the signal. Figure 3d shows the PSD of the CPM-PSWF signal under different time-bandwidth products C. The results indicate that the main lobe bandwidth will gradually widen with the increase of the time-bandwidth product C, so the signal bandwidth can be affected by changing the C. The smaller the C, the lower the power spectrum sidelobe of the modulation signal, and the faster the out-of-band attenuation, this is also the unique advantage of CPM-PSWF compared with traditional CPM signals. However, too small a C value may lead to a decrease in code tracking performance and anti-multipath capability.

The design of the signal system can only be the result of comprehensively weighing all aspects of the system performance, and it is impossible to achieve comprehensive optimization. The main purpose of this paper is to optimize the compatibility and navigation performance of the S-band signal. Considering the strict bandwidth constraint of the S-band and the complexity of CPM-PSWF implementation, this paper proposes a CPM-PSWF signal with $f_c = 8 \times 1.023\text{MHz}$, $M = 2$, $L = 2$, $h = 1.5$, and $C = 6$, denoted as BM2PSWF(8), for the Compass system S-band.

3 Performance evaluation criteria

Evaluating the performance of satellite navigation signals is an essential means of designing and analysing navigation schemes. In this section, the basic introduction and mathematical model of the code tracking accuracy, anti-jamming ability, anti-multipath ability, and compatibility are given.

3.1 Code tracking performance

Observation of the pseudocode and carrier phase is the basis of GNSS receiver positioning and ranging. Accurate tracking of pseud-code is the premise of pseudocode ranging, so code tracking performance is a critical factor in the design of navigation signals. The Gabor bandwidth and code tracking error are essential technical indicators to evaluate the code tracking performance. The Cramer-Rao Lower Bound (CRLB) gives the best tracking accuracy theoretically, and the CRLB is closely related to the Gabor bandwidth.

When only Gaussian white noise interference is considered, the standard deviation of the code tracking error of the coherent early-late processing (CELP) code tracking loop can be expressed as [40]:

$$\delta_{\text{CELP}} = \gamma \sqrt{\frac{B_L(1 - 0.5B_L T_i) \int_{-B_r/2}^{B_r/2} G_s(f) \sin^2(\pi f \nu) \mathrm{d}f}{(2\pi)^2 \frac{C_s}{N_0} \left(\int_{-B_r/2}^{B_r/2} f G_s(f) \sin(\pi f \nu) \mathrm{d}f \right)^2}} \tag{7}$$

where γ is $3 \times 10^8 \text{m/s}$, B_L denotes the loop bandwidth of a single sideband, T_i represents the coherent integration time, B_r is the prefiltering bandwidth of the receiver, ν denotes the interval between early and late correlators, $G_s(f)$ refers to the normalized PSD of the signal, and C_s/N_0 is the carrier-to-noise ratio (CNR).

In the case of Gaussian white noise, the code tracking error variance of the CELP code tracking loop can approach the CRLB when a very small interval is used. At the same time, $B_L T_i$ can be ignored because its weight is far less than 1. When the correlation interval ν tends to 0, using the property of equivalent infinitesimal, the CRLB can be approximately expressed as:

$$\begin{aligned}\lim_{\nu=0}\delta^2_{\mathrm{CELP}} &= \delta^2_{\mathrm{CELB}} \\ &= \frac{B_L\int_{-B_r/2}^{B_r/2} G_s(f)(\pi f\nu)^2 df}{4\pi^2\frac{C_s}{N_0}\left(\int_{-B_r/2}^{B_r/2} G_s(f)\pi f^2\nu df\right)^2} \\ &= \frac{B_L\int_{-B_r/2}^{B_r/2} G_s(f)(\pi f\nu)^2 df}{4\pi^2\frac{C_s}{N_0}\int_{-B_r/2}^{B_r/2} f^2 G_s(f) df}\end{aligned} \tag{8}$$

The Gabor bandwidth f_{Gabor} is defined as:

$$f_{\mathrm{Gabor}} = \sqrt{\int_{-B_r/2}^{B_r/2} f^2 G(f) df} \tag{9}$$

According to Eqs. (8) and (9), the Gabor bandwidth can be used as an important index to measure the lower limit of code tracking errors. The GNSS signal with a larger Gabor bandwidth has a smaller CRLB generated by the code tracking loop, indicating that the signal has better code tracking potential.

3.2 Anti-jamming performance

In terms of anti-jamming, matched spectrum jamming has the greatest impact on navigation signals when the receiver has anti-jamming measures, and narrowband jamming becomes the largest jamming source when the receiver does not have anti-jamming measures. To accurately and effectively evaluate the resistance of navigation signals to these jamming, four indicators are selected: the demodulation anti-narrowband-jamming quality factor, the demodulation anti-matched-spectrum-jamming quality factor, the code tracking anti-narrowband-jamming quality factor, and the code tracking anti-matched-spectrum-jamming quality factor. The signal with larger anti-jamming quality factors has a stronger ability to resist jamming [30].

The expression for the demodulation anti-narrowband-jamming quality factor is:

$$Q_{\mathrm{DemAJNW}} = 10 \times \log_{10}\left[\frac{1}{R_d \times \max[G(f)]}\right](\mathrm{dB}) \tag{10}$$

where R_d denotes the information rate.

The expression for the demodulation anti-matched-spectrum-jamming quality factor is as follows:

$$Q_{\text{DemAJMS}} = 10 \times \log_{10}\left[\frac{1}{R_d \times \int_{-B_r/2}^{B_r/2} G^2(f)df}\right](\text{dB}) \tag{11}$$

The expression for the code tracking anti-narrowband-jamming quality factor is as follows:

$$Q_{\text{CTAJNW}} = 10 \times \log_{10}\left[\frac{\int_{-B_r/2}^{B_r/2} f^2 G(f)df}{\max[f^2 G(f)]}\right](\text{dB}) \tag{12}$$

The expression for the code tracking anti-matched-spectrum-jamming quality factor is:

$$Q_{\text{CTAJMS}} = 10 \times \log_{10}\left[\frac{\int_{-B_r/2}^{B_r/2} f^2 G(f)df}{\int_{-B_r/2}^{B_r/2} f^2 G^2(f)df}\right](\text{dB}) \tag{13}$$

3.3 Anti-multipath performance

The multipath effect is one of the reasons for the measurement error of GNSS receivers, which will destroy the symmetry of the correlation function, and cause deviation of the code phase measurement. The multipath error is related to the GNSS modulation method, so anti-multipath ability analysis has become an important reference for GNSS signal design. At present, the multipath error envelope and the average multipath error are two technical indices used to measure the anti-multipath ability of a signal. The multipath error envelope reflects the sensitivity of a code tracking loop to multipath signals with different parameters. When only one multipath signal exists, the multipath error envelope of the coherent code tracking loop is [41]:

$$\xi_\tau \approx \frac{\pm\tilde{a}_1 \int_{-B_r/2}^{B_r/2} G_s(f)\sin(\pi f \nu)\sin(2\pi f \tau_\varepsilon)df}{2\pi \int_{-B_r/2}^{B_r/2} f G_s(f)\sin(\pi f \nu)(1 \pm \tilde{a}_1 \cos(2\pi f \tau_\varepsilon)df} \tag{14}$$

where $\tilde{a}_1 = a_1/a_0$ represents the ratio of the multipath signal amplitude to the direct signal amplitude, a_1 and a_0 represent the multipath amplitude and direct signal amplitude, respectively, and τ_ε is the delay between the multipath signal and the direct signal. When the phase difference between the multipath signal and the direct signal is 0° and 180°, the symbol $\pm$ is $'+'$ and $'-'$, respectively.

The average multipath error can reflect the overall level of multipath error within the delay range, which is the cumulative average of the multipath error envelope varying with the multipath delay. The relationship between the average multipath error and the multipath error envelope can be expressed as:

$$\xi_a(\tau_\chi) \approx \frac{1}{\tau_\chi}\int_0^{\tau_\chi}\left[\frac{abs\left(\xi_\tau(\tau_\varepsilon)|\tilde{\phi}_1{=}0^\circ\right){+}abs\left(\xi_\tau(\tau_\varepsilon)|\tilde{\phi}_1{=}\ 180^\circ\right)}{2}\right]d\tau_\varepsilon \tag{15}$$

where $\xi_a(\tau_\chi)$ denotes the average multipath error of the multipath delay in the range of $[0, \tau_\chi]$, $\xi_\tau(\tau_\varepsilon)|\tilde{\phi}_1{=}0^\circ$ and $\xi_\tau(\tau_\varepsilon)|\tilde{\phi}_1{=}\ 180^\circ$ represent the multipath error when the phase difference between the multipath signal and the direct signal is 0° and 180°, and the multipath delay is τ_ε.

3.4 Compatibility

The IRNSS has broadcasted BPSK(1) and BOCs(5,2) in the S-band as civil and authorized signals, respectively [14, 22]. Galileo proposed BPSK(1), BPSK(4), BPSK(8), and CBOC(6,1,1/11) as S-band candidate navigation signals [20]. Globalstar uses the S-band as the downlink between the satellite and the user terminal, with a centre frequency of 2491.75 MHz [15]. Moreover, multibeam antennas are used to realize frequency reutilization in Globalstar. In each beam, the 16.5 MHz bandwidth of the S-band is divided into 13 frequency division multiplexing (FDM) channels, and the bandwidth of each channel is 1.23 MHz. Code division multiple access is implemented by using a spreading code with a rate of 1.2288 Mc/s in each FDM channel. In addition, the Globalstar signal needs to be filtered by a Nyquist square-root-raised-cosine filter before carrier modulation, and the expression of the Globalstar signal PSD of each beam is:

$$G_{\text{GLOB}}(f) = \sum_{k=-6}^{6} G_{\text{SRRC}}^{k}(f) \tag{16}$$

where the PSD of the th FDM channel is expressed as:

$$G_{\text{SRRC}}^{k} = \begin{cases} 1, & \left|f - kB_f\right| \leq \frac{f_c}{2}(1-\rho) \\ 0, & \left|f - kB_f\right| \leq \frac{f_c}{2}(1+\rho) \\ \mu(f), & \frac{f_c}{2}(1-\rho) \leq \left|f - kB_f\right| \leq \frac{f_c}{2}(1+\rho) \end{cases} \tag{17}$$

with:

$$\mu(f) = \frac{1}{2}\left(1 + \cos\left(\frac{\pi}{\rho f_c}\left(|f| - \frac{(1-\rho)f_c}{2} - kB_f\right)\right)\right) \tag{18}$$

where the roll-off coefficient ρ is 0.2, the chip rate f_c is 1.2288 MHz, and the FDM channel bandwidth B_f is 1.23 MHz.

Figure 4 depicts the PSD of the S-band signals of the IRNSS, Galileo, and Globalstar systems. It is not difficult to find that the spectrum aliasing between signals is very serious in the S-band with limited bandwidth resources. Therefore, when designing a new S-band signal, it is necessary to analyse the compatibility between existing and candidate signals in the same frequency band.

ITU-RM. 1831 describes a compatibility assessment methodology for the RNSS system [42]. This methodology takes the effective carrier-to-noise ratio degradation as the main parameter for GNSS signal interference evaluation and coordination. However, the effective carrier-to-noise ratio degradation is influenced by multiple factors, such as the satellite layout, user location, and signal system, and the calculation is complex and cannot be quickly solved. Therefore, this paper uses the spectral separation coefficient (SSC) and code tracking spectral separation coefficient (CTSSC) to evaluate the compatibility of satellite navigation signals.

As an important part of the effective carrier-to-noise ratio degradation in the acquisition phase, the spectral separation coefficient reflects the interference and overlap

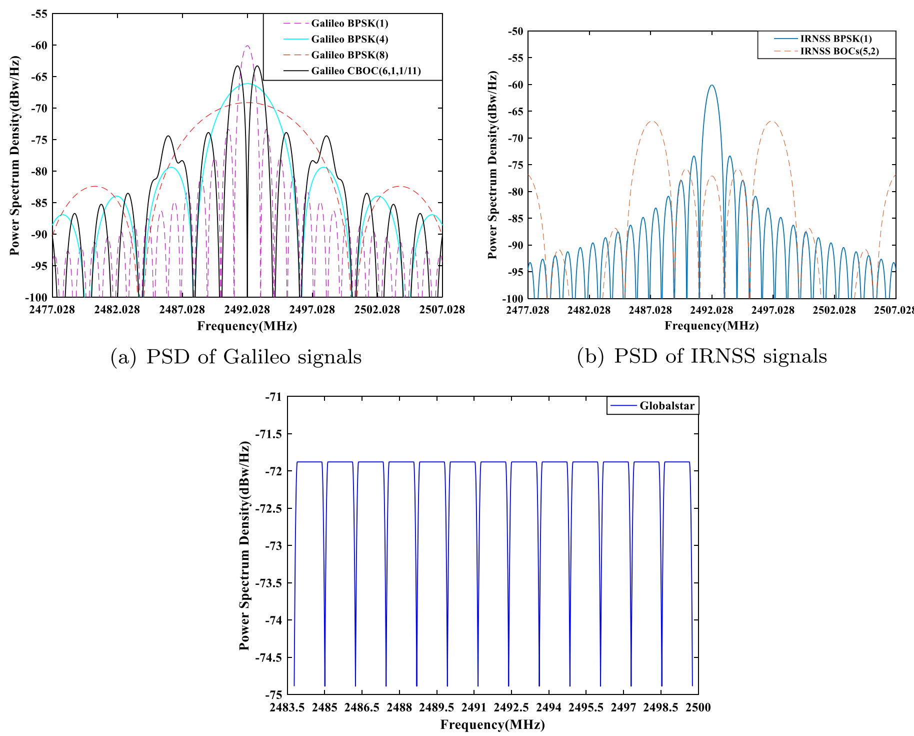

(a) PSD of Galileo signals

(b) PSD of IRNSS signals

(c) PSD of Globalstar signals

Fig. 4 Power spectrum density of GNSS signals in the S-band

degree of the interference signal and the desired signal [43]. The SSC can be expressed as follows:

$$K_{\text{ls}} = \int_{-B_r/2}^{B_r/2} G_l(f) G_s(f) df \tag{19}$$

where $G_l(f)$ denotes the normalized PSD of the interference signal, and $G_s(f)$ represents the normalized PSD of the desired signal.

The code tracking spectral sensitivity coefficient effectively reflects the impact of the interference signal on the code tracking performance of the desired signal [44]. The CTSSC is defined as:

$$\chi_{\text{ls}} = \frac{\int_{-B_r/2}^{B_r/2} G_l(f) G_s(f) \sin^2(\pi f \nu) df}{\int_{-B_r/2}^{B_r/2} G_s(f) \sin^2(\pi f \nu) df} \tag{20}$$

4 Performance evaluation results for the compass S-band

This section comprehensively evaluates the navigation performance of the proposed BM2PSWF(8) signal and other Compass S-band candidate signals based on the analysis of the PSD, code tracking performance, anti-multipath ability, anti-jamming ability, and compatibility, providing a valuable reference for future Compass S-band signal design.

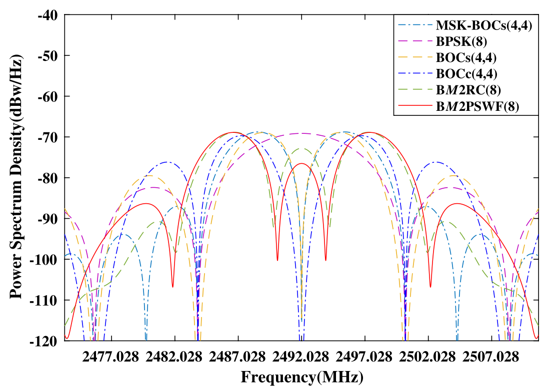

Fig. 5 PSD of candidate signals in the Compass S-band

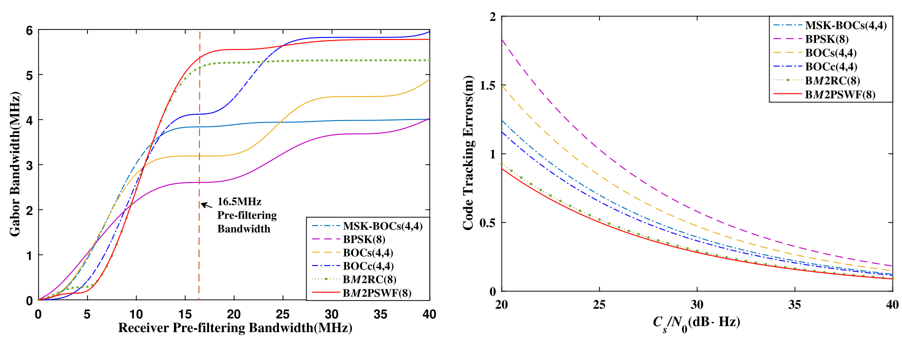

(a) Gabor bandwidth (b) Code tracking errors of coherent processing

Fig. 6 Code tracking performance of each candidate signals in the S-band

4.1 PSD of compass S-band

MSK-BOCs(4,4), BOCc(4,4), BOCs(4,4), BPSK(8), and B*M*2RC(8) have been proposed as candidate schemes for the S-band of the Compass system [24, 31]. Figure 5 illustrates the PSD of the above signals and B*M*2PSWF(8) signal. Compared with other candidate signals, the proposed B*M*2PSWF(8) signal has similar main lobe width, which can make full use of the limited bandwidth resources of the S-band. Moreover, the B*M*2PSWF(8) signal can concentrate more high-frequency components at the edge of the available bandwidth, indicating that B*M*2PSWF(8) has better code tracking potential. In addition, B*M*2PSWF(8) has similar out-of-band sidelobe characteristics to B*M*2RC(8). Compared with MSK-BOCs(4,4), BPSK(8), BOCs(4,4), and BOCc(4,4), B*M*2PSWF(8) has faster sidelobe attenuation, which can effectively reduce the impact on the adjacent frequency band signal.

4.2 Code tracking performance

Figure 6 compares the code tracking performance of S-band candidate signals, where the coherent integration time T_i is 1 ms, the correlation interval ν is 0.1 chip, the loop bandwidth B_L is 1 Hz, and the carrier-to-noise ratio C_s/N_0 is 20–50 dB Hz. Figure 6a shows that when the receiving bandwidth B_r exceeds 12.5 MHz, the Gabor bandwidth of the B*M*2PSWF(8) signal begins to be larger than that of the other candidate signals, and the B*M*2PSWF(8) signal has the maximum Gabor bandwidth when the receiving bandwidth is 16.5 MHz. At the same time, under the available bandwidth of 16.5 MHz in the S-band, its Gabor bandwidth is close to the maximum, which can maximize the code tracking potential.

Figure 6b compares the code tracking errors of each candidate signal at the receiving bandwidth of 16.368 MHz. Similar to the above analysis results, the B*M*2PSWF(8) signal has higher code tracking accuracy. The B*M*2PSWF(8) signal can save 0.35 dB, 2.3 dB, 2.9 dB, 4.5 dB, and 6.25 dB of carrier power compared with B*M*2RC(8), BOCc(4,4), MSK-BOCs(4,4), BOCs(4,4), and BPSK(8) under a 0.2 m code tracking error. Gabor bandwidth and code tracking error curves show that compared with other Compass S-band candidate signals, the B*M*2PSWF(8) has the best code tracking performance and high precision code tracking potential.

4.3 Anti-jamming performance analysis

The anti-jamming performance of each S-band candidate signal is calculated in Table 2, where B_r and R_d are 16.368 MHz and 50 bps, respectively. From the demodulation anti-narrowband-jamming aspect, the anti-jamming quality factor of each candidate signal is very close. B*M*2PSWF(8) and B*M*2RC(8) perform best in demodulation anti-matched-spectrum-jamming, while MSK-BOCs(4,4) performs slightly poorly. BPSK(8) has the best anti-jamming performance while B*M*2PSWF(8) and B*M*2RC(8) have poor performance in code tracking anti-narrowband-jamming. BPSK(8) has the best anti-jamming performance in code tracking anti-matched-spectrum-jamming. In general, the difference in anti-jamming performance among candidate signals is very small, indicating that they have similar anti-jamming performance.

4.4 Anti-multipath performance analysis

Figure 7 compares the anti-multipath ability of the S-band candidate signals in the presence of a single multipath signal, where $\tilde{a}_1$ is -6 dB, the receiving bandwidth B_r is 16.368 MHz, and the correlation interval ν is 0.1 chip. Figure 7a illustrates the variation in the multipath error envelope of each candidate signals with the multipath delay. The multipath error envelope of almost all candidate signals reaches a peak when the multipath delay is approximately 22 m. After that, as the multipath delay increases, the multipath error gradually decreases and converges to a small value at approximately 80 m. The multipath error envelope amplitude of the B*M*2PSWF(8) signal is the smallest and the convergence speed is the fastest.

Table 2 The anti-jamming performance of each candidate signal in the S-band

Merit factors	B*M*2PSWF(8)	B*M*2RC(8)	BOCs(4,4)	BOCc(4,4)	BPSK(8)	MSK-BOCs(4,4)
$Q_{DemAJNW}$	51.9045	51.8672	51.9276	52.6869	52.1400	51.7845
$Q_{DemAJMS}$	56.5060	56.5612	53.9370	55.3525	53.9137	53.1460
Q_{CTAJNW}	65.1779	65.0385	67.8803	67.8263	69.1297	68.3022
Q_{CTAJMS}	70.1958	70.2716	70.7160	71.0772	72.8167	70.5077

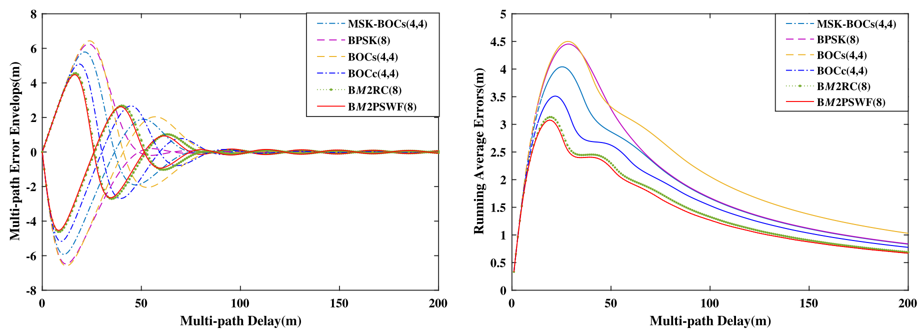

(a) Multipath error envelope (b) Average multipath error envelope

Fig. 7 Anti-multipath performance of each candidate signals in the S-band

Figure 7b depicts the variation in the average multipath error with the multipath delay. The anti-multipath ability of the BM2PSWF(8) signal is slightly better than that of the other candidate signals as a whole. The maximum average multipath error of BM2PSWF(8) is lower than those of BM2RC(8), BOCc(4,4), MSK-BOCs(4,4), BOCs(4,4), and BPSK(8), which are approximately 0.06 m, 0.44 m, 0.96 m, 1.42 m, and 1.37 m. Therefore, the anti-multipath ability of the BM2PSWF(8) signal is more advantageous for the S-band candidate signal.

4.5 Compatibility performance analysis

Table 3 reports the SSCs of the Galileo, IRNSS, and Globalstar system signals as the desired signal and each S-band candidate signal as the interference signal, where $\text{Globalstar}_{max}^{single}$ is the single FDM signal corresponding to the maximum SSC, the receiving bandwidth of the Galileo and IRNSS signals are 16.368 MHz, and the receiving bandwidth of the Globalstar signal is 1.23 MHz. Table 3 indicates that when BPSK(1) is the desired signal, the interference of BM2PSWF(8) is significantly smaller than that of BM2RC(8). The interference caused by BM2PSWF(8) for BPSK(4), BPSK(8), and CBOC(6,1,1/11) is significantly smaller than that caused by the other candidate signals except for BOCc(4,4). This is because BOCc(4,4) has fewer low-frequency components in the bandwidth range, which will result in relatively low spectral efficiency or high spectral leakage.

The compatibility between the BM2PSWF(8) signal and BOCs(5,2) is slightly worse than that of the other candidate signals, but it is still acceptable. The interference introduced by BM2PSWF(8) in the Globalstar acquisition phase is less than that introduced by BM2RC(8), BPSK(8), and MSK-BOCs(4,4), but greater than that introduced by BOCc(4,4) and BOCs(4,4). It can be seen that in the capture phase, BM2PSWF(8) has a comprehensive improvement in the performance of inter-system compatibility compared with BM2RC(8), especially the compatibility with BPSK modulation is more obviously, and the maximum can be increased by nearly 3.5 dB.

The CTSSCs of the Galileo system and the IRNSS system signals as the desired signals and the Compass S-band candidate signals as the interference signals are shown in Fig. 8. As shown in Fig. 8a, BM2PSWF(8) has the least influence on the code tracking performance of BPSK(1) when the interval ν is small. As the interval increases, the CTSSC is stable at approximately -77 dB, and the compatibility of BM2PSWF(8) is better

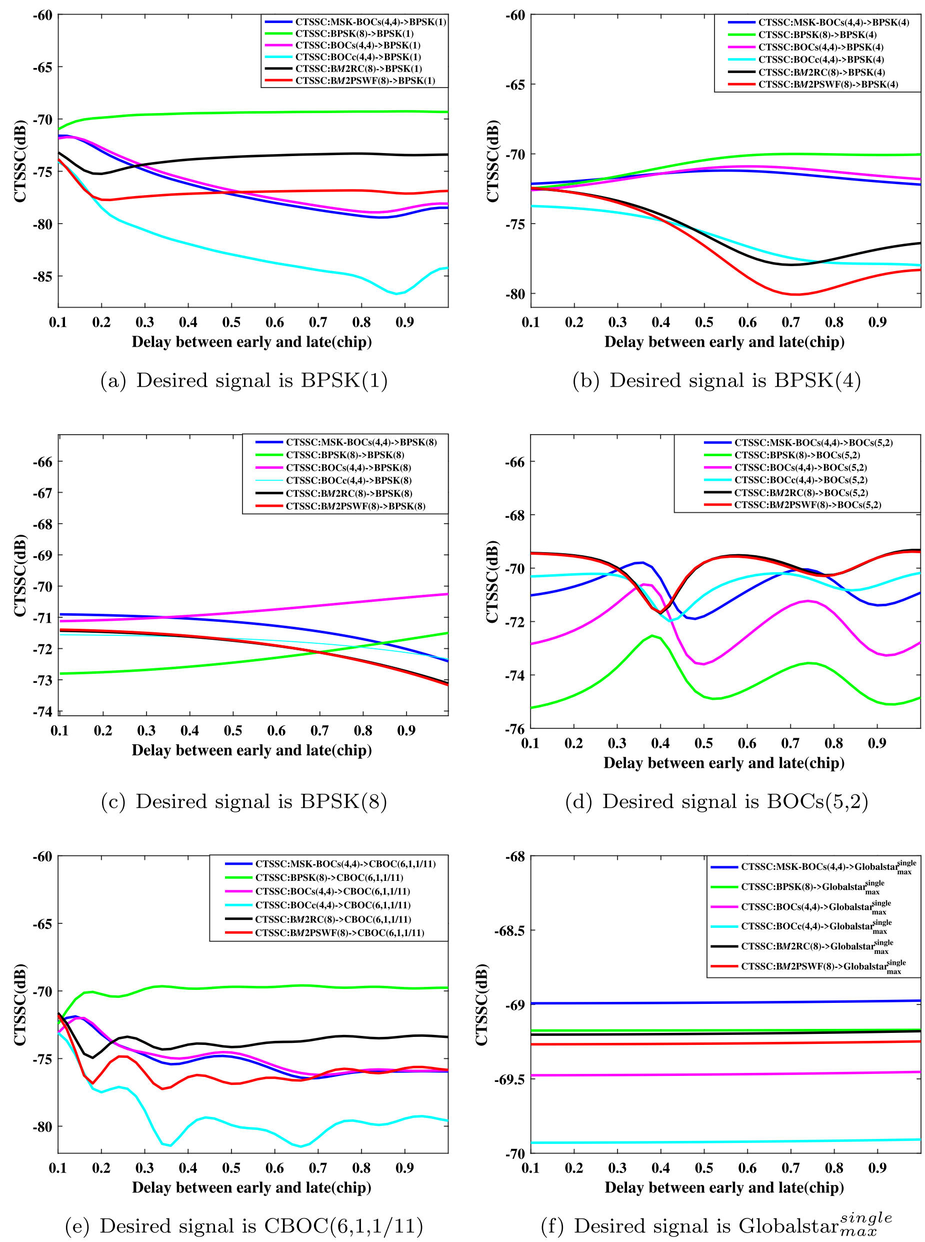

(a) Desired signal is BPSK(1)
(b) Desired signal is BPSK(4)
(c) Desired signal is BPSK(8)
(d) Desired signal is BOCs(5,2)
(e) Desired signal is CBOC(6,1,1/11)
(f) Desired signal is Globalstar$^{single}_{max}$

Fig. 8 CTSSC of GNSS signals in the S-band

Table 3 SSC between the desired signal and the candidate signal

SSC(dB)	B*M*2PSWF(8)	B*M*2RC(8)	BOCs(4,4)	BOCc(4,4)	BPSK(8)	MSK-BOCs(4,4)
BPSK(1)	−76.7564	−73.1884	−79.9343	−86.0651	−69.3153	−80.3243
BPSK(4)	−77.8040	−74.9696	−73.9122	−80.0727	−69.9253	−74.3046
BPSK(8)	−75.4026	−74.3516	−72.1678	−75.2494	−70.9034	−72.0851
BOCs(5,2)	−70.6838	−70.6216	−73.1024	−71.3411	−74.9812	−71.6039
CBOC(6,1,1/11)	−76.1212	−73.8356	−75.3637	−79.3691	−70.0725	−75.4980
Globalstar$^{single}_{max}$	−80.3037	−80.2225	−80.4980	−80.9733	−80.2941	−80.0350

than that of BM2RC(8) and BPSK(8). Figure 8b shows that compared with the other BDS candidate signals, the BM2PSWF(8) signal introduces the least interference in the BPSK(4) tracking phase.

The influences of BM2PSWF(8) and BM2RC(8) on the code tracking accuracy of the BPSK(8) signal are very close, which are significantly better than those of MSK-BOCs(4,4), BOCs(4,4), and BOCc(4,4), as shown in Fig. 8c. Figure 8d indicates that if the desired signal is BOCs(5,2), then the compatibility of BM2PSWF(8) is similar to that of the BM2RC(8) signal and slightly worse than that of the other candidate signals. Figure 8e shows that the compatibility between the BM2PSWF(8) signal and CBOC(6,1,1/11) is significantly better than that of the other candidate signals except for BOCc(4,4). Figure 8f shows that the interference introduced by BM2PSWF(8) in the Globalstar tracking phase is less than that introduced by BM2RC(8), BPSK(8), and MSK-BOCs(4,4), but greater than that introduced by BOCc(4,4) and BOCs(4,4). It is easy to see that in the tracking phase, when the desired signal is BPSK(1), BPSK(4), CBOC(6,1,1/11), BM2PSWF(8) compared with BM2RC(8), the introduced interference is significantly reduced and the compatibility is better. From the above analysis of the SSC and CTSSC, the BM2PSWF(8) signal has better in-band compatibility than the BM2RC(8) signal in both the acquisition and tracking stages.

5 Conclusion

The importance of S-band navigation due to increased L-band congestion is gradually being highlighted. Compatibility and navigation performance are important issues to be considered in the design of new S-band signals. In this paper, CPM-PSWF is proposed as the S-band signal modulation method of the Compass system. PSWF with excellent time-frequency energy concentration and flexible time-band product is used as the frequency pulse function of CPM to improve the compatibility and navigation performance of existing candidate signals. Through simulation analysis of key modulation parameters, the BM2PSWF(8), $h = 1.5$, $C = 6$ signal is selected as the candidate navigation signal of the S-band. Simulation results show that compared with S-band candidate signals such as BM2RC(8), BOCc(4,4), MSK-BOCs(4,4), BOCs(4,4) and BPSK(8), the proposed signal has excellent spectral characteristics, larger Gabor bandwidth, higher code tracking accuracy, lower average multipath error, and similar anti-multipath performance. In terms of compatibility, compared with other candidate signals except for BOCc(4,4), the proposed signal has the lowest mutual interference with most signals of IRNSS, Globalstar, and Galileo systems in both the acquisition and tracking stages. In addition, the modulation scheme can provide a new idea and feasibility demonstration for the signal design of the Compass system.

Acknowledgements
Not applicable.

Author contributions
Mingming Xie is responsible for conceptualization, method research, program simulation, writing, and editing. Rui Xue conducted data collation, writing, first draft preparation, and review. All authors read and approved the final manuscript.

Funding
This paper was supported in part by the National Natural Science Foundation of China (No. 61873070), the Heilongjiang Provincial Natural Science Foundation of China (No. LH2020F018), the Fundamental Research Funds for the Central Universities (No. 3072022QBZ0803).

Availability of data and materials
Please contact author for data requests.

Declarations

Ethics approval and consent to participate
Not applicable.

Consent for publication
The picture materials quoted in this article have no copyright requirements, and the source has been indicated.

Competing interests
The authors declare that they have no competing interests.

Received: 26 April 2023 Accepted: 18 August 2023
Published online: 28 August 2023

References

1. J.W. Betz, Signal structures for satellite-based navigation: Past, present, and future. In: Proceedings of the ION 2013 Pacific PNT Meeting, pp. 131–137 (2013)
2. Y. Gao, Z. Yao, M. Lu, High-precision unambiguous tracking technique for bds b1 wideband composite signal. Navigation **67**(3), 633–650 (2020)
3. H. Shin, K. Han, J.-H. Won, Development of end-to-end numerical simulator for next generation gnss signal design. J. Position. Navig. Timing **8**(4), 153–164 (2019)
4. K. Wang, S. Zhang, J. Wang, Feasibility of using an s-band gnss carrier by comparing with l and c bands. Adv. Space Res. **66**(9), 2232–2244 (2020)
5. B.-M. Kwon, Y.-S. Shin, K.-S. Ma, J.-G. Ju, K.-M. Ji, Radio frequency interference on the gnss receiver due to s-band signals. J. Korean Soc. Aeronaut. Space Sci. **47**(5), 388–396 (2019)
6. K. Han, Y.-J. Song, J.-H. Won, A study on the effects of out-of-band interference on rnss receivers in s-band. In: Proceedings of the 34th international technical meeting of the satellite division of the institute of navigation (ION GNSS+ 2021), pp. 796–802 (2021)
7. G.W. Hein, Status, perspectives and trends of satellite navigation. Satel. Navig. **1**(1), 22 (2020)
8. Z. Yao, M. Lu, Z. Yao, M. Lu, Structure of satellite navigation signals. Next-generation GNSS signal design: theories, principles and technologies, pp. 19–64 (2021)
9. F. Soualle, T. Bey, J. Floch, D. Hurd, M. Notter, C. Mathew, P. Mattos, C. Mongredien, Assessment on the use of s-band for combined navigation and communication. In: Proceedings of the 24th international technical meeting of the satellite division of the institute of navigation (ION GNSS 2011), pp. 1219–1233 (2011)
10. F. Mahbub, S.B. Akash, S.A.K. Al-Nahiun, R. Islam, R.R. Hasan, M.A. Rahman, Microstrip patch antenna for the applications of wlan systems using s-band. In: 2021 IEEE 11th annual computing and communication workshop and conference (CCWC), pp. 1185–1189 (2021). IEEE
11. D.V. Ratnam, T.R. Vishnu, P.B.S. Harsha, Ionospheric gradients estimation and analysis of s-band navigation signals for navic system. IEEE Access **6**, 66954–66962 (2018)
12. S.R. Ammana, M. Sujimol, K.K. Songala, A. Sarma, Advantage of irnss s-band signal for gbas applications in adverse ionospheric storm conditions. Aerosp. Syst. **5**(4), 615–624 (2022)
13. M. Paonni, J.T. Curran, M. Bavaro, J. Fortuny-Guasch, Gnss meta signals: Coherently composite processing of multiple gnss signals. In: Proceedings of the 27th international technical meeting of the satellite division of the institute of navigation (ION GNSS+ 2014), pp. 2592–2601 (2014)
14. S. Thoelert, O. Montenbruck, M. Meurer, Irnss-1a: signal and clock characterization of the indian regional navigation system. GPS Solut. **18**, 147–152 (2014)
15. J.N. Pelton, S. Madry, S. Camacho-Lara, *Handbook of satellite applications* (Springer, New York, 2017)
16. J.-L. Issler, F. Perozans, Y. Tawk, A. Jovanovic, C. Botteron, P.-A. Farine, R. Landry, M. Sahmoudi, V. Dehant, A. Caporali, et al.: Universal-sbas: a worldwide multimodal standard. In: Proceedings ELMAR-2010, pp. 429–444 (2010). IEEE
17. K. Han, S. Lee, M. You, J.-H. Won, A comprehensive evaluation of possible rnss signals in the s-band for the kps. Sensors **22**(6), 2180 (2022)
18. Y. Yang, J. Tang, O. Montenbruck, Chinese navigation satellite systems. Springer handbook of global navigation satellite systems, pp. 273–304 (2017)
19. J.-J. Floch, F. Antreich, M. Meurer, J.-L. Issler, S-band signal design considering interoperability and spectral separation. In: Proceedings of the 23rd international technical meeting of the satellite division of the institute of navigation (ION GNSS 2010), pp. 3349–3358 (2010)
20. I. Mateu, C. Boulanger, J.-L. Issler, L. Ries, J.-A. Avila-Rodriguez, S. Wallner, T. Kraus, B. Eissfeller, P. Mulassano, S. Germaine, et al., Exploration of possible gnss signals in s-band. In: Proceedings of the 22nd International Technical Meeting of the Satellite Division of the Institute of Navigation (ION GNSS 2009), pp. 1573–1587 (2009)
21. E. Sénant, B. Gadat, C. Charbonnieras, S. Roche, M. Aubault, F.-X. Marmet, Tentative new signals and services in upper l1 and s bands for galileo evolutions. In: Proceedings of the 31st International Technical Meeting of the Satellite Division of The Institute of Navigation (ION GNSS+ 2018), pp. 913–942 (2018)
22. N. Nadarajah, A. Khodabandeh, P.J. Teunissen, Assessing the irnss l5-signal in combination with gps, galileo, and qzss l5/e5a-signals for positioning and navigation. GPS Solut. **20**, 289–297 (2016)

23. F. Wang, D. Zeng, R. Li, Study on msk modulation for s-band. In: China Satellite Navigation Conference (CSNC) 2013 Proceedings: satellite navigation signal system, compatibility and interoperability augmentation and integrity monitoring models and methods, pp. 61–69 (2013). Springer
24. P. Qin, The research of the signal in the s frequency band. In: Proceedings of 2013 China satellite navigation conference, Wuhan, China, vol. 1517, p. 15 (2013)
25. D. Huang, H. Leung, X. Huang, Experimental evaluation of predistortion techniques for high-power amplifier. IEEE Trans. Instrum. Meas. **55**(6), 2155–2164 (2006)
26. J. Jeong, D.F. Kimball, M. Kwak, C. Hsia, P. Draxler, P.M. Asbeck, Wideband envelope tracking power amplifiers with reduced bandwidth power supply waveforms and adaptive digital predistortion techniques. IEEE Trans. Microw. Theory Tech. **57**(12), 3307–3314 (2009)
27. J. Ji, Y. Liu, W. Chen, D. Wu, H. Lu, J. Zhang, A novel signal design and performance analysis in navcom based on leo constellation. Sensors **21**(24), 8235 (2021)
28. J.B. Anderson, T. Aulin, C.-E. Sundberg, *Digital phase modulation* (Springer, New York, 2013)
29. L. Wang, X. Huang, J. Li, X. Tang, F. Wang, Proposal of spread spectrum msk for bds rdss signal modulation. IET radar, sonar and navigation **14**(6), 870–878 (2020)
30. R. Xue, Y. Sun, D. Zhao, Cpm signals for satellite navigation in the s and c bands. Sensors **15**(6), 13184–13200 (2015)
31. Y. Sun, R. Xue, D. Zhao, D. Wang, Radio frequency compatibility evaluation of s band navigation signals for future beidou. Sensors **17**(5), 1039 (2017)
32. F. Ma, X. Zhang, J. Hu, P. Li, L. Pan, S. Yu, Z. Zhang, Frequency design of leo-based navigation augmentation signals for dual-band ionospheric-free ambiguity resolution. GPS Solut. **26**(2), 53 (2022)
33. Y. Sun, Optimal parameter design of continuous phase modulation for future gnss signals. IEEE Access **9**, 58487–58502 (2021)
34. D.-W. Yang, C.-H. Liu, L. Zhang, Cpm-pswfs signal demodulation method based on waveform coherence. In: 2020 IEEE 20th international conference on communication technology (ICCT), pp. 1237–1241 (2020). IEEE
35. D. Slepian, H.O. Pollak, Prolate spheroidal wave functions, Fourier analysis and uncertainty-i. Bell Syst. Tech. J. **40**(1), 43–63 (1961)
36. T. Takami, U.D. Nielsen, J.J. Jensen, Estimation of autocorrelation function and spectrum density of wave-induced responses using prolate spheroidal wave functions. J. Mar. Sci. Technol. **26**, 772–791 (2021)
37. A. Osipov, V. Rokhlin, H. Xiao et al., Prolate spheroidal wave functions of order zero. Springer Ser. Appl. Math. Sci **187**, (2013)
38. T. Aulin, N. Rydbeck, C.-E. Sundberg, Continuous phase modulation-part ii: partial response signaling. IEEE Trans. Commun. **29**(3), 210–225 (1981)
39. B. Parr, B. Cho, K. Wallace, Z. Ding, A novel ultra-wideband pulse design algorithm. IEEE Commun. Lett. **7**(5), 219–221 (2003)
40. J.W. Betz, K.R. Kolodziejski, Generalized theory of code tracking with an early-late discriminator part i: lower bound and coherent processing. IEEE Trans. Aerosp. Electron. Syst. **45**(4), 1538–1556 (2009)
41. R. Xue, Q.-M. Cao, Q. Wei, A flexible modulation scheme design for c-band gnss signals. Math. Probl Eng. **2015**, (2015)
42. M.1831: A coordination methodology for RNSS inter-system interference estimation (2015). Accessed 19 Apr 2023, https://www.itu.int/rec/R-REC-M.1831-1-201509-I/en
43. J.W. Betz, D.B. Goldstein, Candidate designs for an additional civil signal in gps spectral bands. In: Proceedings of the 2002 national technical meeting of the institute of navigation, pp. 622–631 (2002)
44. F. Soualle, T. Burger, Radio frequency compatibility criterion for code tracking performance. In: Proceedings of the 20th international technical meeting of the satellite division of the institute of navigation (ION GNSS 2007), pp. 1201–1210 (2007)

Publisher's Note